Structural determinants of multimerization and dissociation in 2-Cys peroxiredoxin chaperone function

Downloaded from: https://research.chalmers.se, 2024-04-24 23:10 UTC

Citation for the original published paper (version of record):
Troussicot, L., Burmann, B., Molin, M. (2021). Structural determinants of multimerization and dissociation in 2-Cys peroxiredoxin chaperone function. Structure, 29(7): 640-654. http://dx.doi.org/10.1016/j.str.2021.04.007

N.B. When citing this work, cite the original published paper.

research.chalmers.se offers the possibility of retrieving research publications produced at Chalmers University of Technology. It covers all kind of research output: articles, dissertations, conference papers, reports etc. since 2004. research.chalmers.se is administrated and maintained by Chalmers Library

(article starts on next page)

CellPress
OPEN ACCESS

Structure

Review

Structural determinants of multimerization and dissociation in 2-Cys peroxiredoxin chaperone function

Laura Troussicot,[1,2] Björn M. Burmann,[1,2,4,*] and Mikael Molin[1,3,4,*]
[1]Department of Chemistry and Molecular Biology, University of Gothenburg, 405 30 Göteborg, Sweden
[2]Wallenberg Centre for Molecular and Translational Medicine, University of Gothenburg, 405 30 Göteborg, Sweden
[3]Department of Biology and Biological Engineering, Chalmers University of Technology, 405 30 Göteborg, Sweden
[4]These authors contributed equally
*Correspondence: bjorn.marcus.burmann@gu.se (B.M.B.), mikael.molin@chalmers.se (M.M.)
https://doi.org/10.1016/j.str.2021.04.007

SUMMARY

Peroxiredoxins (PRDXs) are abundant peroxidases present in all kingdoms of life. Recently, they have been shown to also carry out additional roles as molecular chaperones. To address this emerging supplementary function, this review focuses on structural studies of 2-Cys PRDX systems exhibiting chaperone activity. We provide a detailed understanding of the current knowledge of structural determinants underlying the chaperone function of PRDXs. Specifically, we describe the mechanisms which may modulate their quaternary structure to facilitate interactions with client proteins and how they are coordinated with the functions of other molecular chaperones. Following an overview of PRDX molecular architecture, we outline structural details of the presently best-characterized peroxiredoxins exhibiting chaperone function and highlight common denominators. Finally, we discuss the remarkable structural similarities between 2-Cys PRDXs, small HSPs, and J-domain-independent Hsp40 holdases in terms of their functions and dynamic equilibria between low- and high-molecular-weight oligomers.

INTRODUCTION

Peroxiredoxins (PRDXs) are highly abundant ubiquitous peroxidases expressed at various intracellular locations in organisms from all biological kingdoms (Harper et al., 2017). Recent studies have revealed a large range of crucial auxiliary functions for PRDXs (Angelucci et al., 2013; Barranco-Medina et al., 2009; Bodvard et al., 2017; Castro et al., 2011; Hanzen et al., 2016; Jang et al., 2004; Molin et al., 2011; Moon et al., 2005; Neumann et al., 2009; Roger et al., 2020; Teixeira et al., 2015), including key roles as cellular regulators of cysteine-based redox signaling (Roger et al., 2020; Stocker et al., 2018) and as molecular chaperones (Hanzen et al., 2016; Teixeira et al., 2019). Peroxiredoxins thus contribute to cellular well-being in at least three complementary ways: managing reactive oxygen species (ROS), controlling ROS signaling, and preventing protein aggregate accumulation. Understanding the molecular details of these diverse sets of functions requires a detailed structural understanding of PRDXs.

Herein, we focus on structural aspects of the typical 2-Cys PRDXs and on structure-function relationships underlying their chaperone function—features still poorly characterized and only partially understood. Within this sub-class of PRDXs the basic active unit is a dimer that, during the catalytic cycle, is linked by disulfide bonds between two catalytically cysteines, C_P on one protomer and C_R of the adjacent protomer (Flohe and Harris, 2007).

We highlight the current understanding of structure-function relationships in 2-Cys PRDXs at atomic resolution. Furthermore, we discuss the so far best characterized cases of PRDXs chaperone function and draw attention to the striking similarities between PRDXs, small HSPs (heat shock proteins), and J-domain-independent Hsp40 holdases, a feature we propose relates to the fundamental basis of PRDX chaperone function. Finally, we provide an outlook on important questions to be addressed in the future in this highly dynamic research field. For more general overviews of the functional aspects of the different PRDX families as well as their respective structural features, we refer the reader to several excellent reviews (Cho et al., 2010; Flohe and Harris, 2007; Hall et al., 2009; Karplus and Hall, 2007; Rhee, 2016; Rhee et al., 2005, 2007; Wood et al., 2003b).

GENERAL CHARACTERISTICS OF MOLECULAR CHAPERONES

To ensure the integrity and function of the proteome, all living cells have to control the protein folding process, i.e., the self-assembly of an unfolded polypeptide chain into its functional three-dimensional conformation (Anfinsen, 1973; Balchin et al., 2016; Hartl et al., 2011; Kim et al., 2013; Mayer and Bukau, 2005). Within the cellular context, specific proteins guide the unfolded polypeptide toward its native functional state—they chaperone them. Molecular chaperones generally prevent aggregation by interacting with clients through unfolded and exposed

 © 2021 The Author(s). Published by Elsevier Ltd.
This is an open access article under the CC BY license (http://creativecommons.org/licenses/by/4.0/).

polypeptide segments (Kim et al., 2013). Importantly, chaperones only guide the transition of the client toward its folded form, without being a component of the functional client. Chaperones form a vast cellular network of diverse proteins accompanying and supporting newly synthesized proteins on their path to their functional state or their sub-cellular environment (Balchin et al., 2016; Hartl et al., 2011; Mayer and Bukau, 2005).

Members of the molecular chaperone family are known as heat shock proteins (HSPs), as they are upregulated under cellular stress conditions to cope with increasing concentrations of aggregation-prone folding intermediates. Many chaperones convert the energy released by ATP hydrolysis to switch between different functional states and exert force on their clients (foldases), whereas others can fulfill their functions in an ATP-independent manner (holdases) (Balchin et al., 2016; Hartl et al., 2011). Holdases bind unfolded and partially folded clients for sufficient time to prevent them from aggregating (Burmann and Hiller, 2015; Saibil, 2013). Whereas their functions are ATP independent, they may be combined with chaperones mediating ATP hydrolysis in some complexes, as for example, in the Hsp70/Hsp40 system. On a structural level holdase chaperone function is intimately connected to oligomerization (Haslbeck and Vierling, 2015; Haslbeck et al., 2019; Mogk et al., 2019). Changes in oligomeric states have together with order to disorder transitions, been shown to be important for client interactions of holdase chaperones (Mas et al., 2020). In the case of small HSPs, oligomerization has been hypothesized to maintain chaperone-active monomers in an inactive storage form, insensitive to aggregation and ready to be released upon specific stimuli (Alderson et al., 2019; Haslbeck et al., 1999). Among the "foldase" chaperones the Hsp70s, which enable folding of client proteins together with their obligate J-protein/Hsp40 co-chaperones, can be found as well as chaperonins (Hsp60s, GroEL/ES in *E. coli*), which act as folding chambers formed by one or multiple ring structures (Balchin et al., 2016; Hartl et al., 2011; Saibil, 2013). Hsp70s use an ATPase cycle to bind and release clients. In the ATP-bound state, substrates can access the substrate-binding domain of the Hsp70s, whereas both substrate binding and the Hsp40 J-domain stimulate ATP hydrolysis resulting in clients being trapped and partially unfolded. Specific nucleotide-exchange factors subsequently reinstate ATP in the nucleotide-binding domain upon which clients may be released and enabled to fold correctly. The best understood function of the J-proteins (Hsp40s) is their role in regulating the Hsp70 ATPase cycle (Craig and Marszalek, 2017). Through the ability of the J-domain to stimulate the weak intrinsic ATPase activity of the Hsp70s, J-proteins are involved in a wide variety of Hsp70-dependent chaperone functions in protein folding, transport, and degradation (Balchin et al., 2016; Hartl et al., 2011).

Due to the disordered nature of unfolded or partially folded clients, substrates need to be bound in a highly dynamic fashion, a fact that has prevented structural characterization of their substrate-binding mechanisms for a long time (Burmann and Hiller, 2015; Burmann et al., 2013; Jiang et al., 2019; Morgado et al., 2017; Sekhar et al., 2018). In particular, details on how chaperones recognize their clients, in which conformational states the clients bind to chaperones, and how clients are subsequently released, are lacking, although protein denaturation and unfolded states seem to be a common theme (Hiller, 2021). Nevertheless, using solution NMR, it was proposed that the *E. coli* holdase chaperones Spy, SurA, and Skp, interact with substrates through locally "frustrated" structural segments or amino acids where movements to minimize the free energy of contact between residues are hampered by mobility constraints (Ferreiro et al., 2014; He and Hiller, 2019). Locally frustrated segments of the client are thought to be recognized by suitable, but biochemically diverse, sequence-unspecific interaction surfaces in the chaperones and client-chaperone interactions are thought to stabilize such client segments. In this way, chaperones adapt to their substrate in a structural and dynamical manner (Burmann and Hiller, 2015).

STRUCTURAL TRANSITIONS IN THE PEROXIREDOXIN PEROXIDASE CATALYTIC CYCLE

The peroxiredoxin catalytic cycle consists of three main steps. In the peroxidation step, the peroxide reacts with the enzyme in its compact fully folded (FF) state, oxidizing the peroxidatic cysteine C_P to a sulfenic acid (C_P-SOH) (Figure 1A). Whereas PRDXs obligately assemble into homodimers, reduced dimers preferentially oligomerize into decamers, a feature that has been noted to increase H_2O_2 reactivity (Nelson et al., 2018). The resolution step is needed to regenerate the reduced protein (Figure 1A). Within the FF state the active site is buried inside a hydrophobic pocket. Therefore, local unfolding of helix α_2 containing the active site is necessary to expose the Cp (LU state) in order for the resolving cysteine C_R from the other subunit of the dimer to react with C_P and form a disulfide bond (Figure 1B). Recent studies suggest that the unfolding of the active site is facilitated by C_P sulfenylation (C_P-SOH) (Kriznik et al., 2020). Resolution leads to the formation of two disulfide bonds linking the two C_P residues within one monomer to the C_R residues in the adjacent monomer in the dimer (Figure 1B). This re-arrangement is accompanied by the dissociation of decamers into dimers (Chae et al., 1994; Rhee et al., 2005). The last step is called recycling and involves regeneration of the PRDX into the reduced FF state by the Trx/TrxR/NADPH system (Hall et al., 2009). Upon local unfolding of the protein, the C_P becomes more accessible for further peroxide molecules to react, possibly leading to hyperoxidation of the C_P to sulfinic (C_P-SO_2H) or sulfonic (C_P-SO_3H) acids, which inactivates peroxidase activity. However, the ATP-dependent sulfinic acid reductase enzyme sulfiredoxin (Srx) may reduce the sulfinic acid (C_P-SO_2H), but not the sulfonic acid (C_P-SO_3H), enabling the PRDX to re-enter the catalytic cycle (Biteau, 2003; Jeong et al., 2012; Jonsson et al., 2005; Rhee et al., 2007; Yang et al., 2002). The Karplus and Poole labs crystallized the first bacterial PRDX, AhpC (Wood et al., 2003a, 2003b), subsequently serving as a blue-print for structural studies of other PRDXs. The crystal structure of a homodimer of AhpC was reported first (PDB: 1HYU), whereas an initial version of a ring-shaped decamer (PDB: 1KYG, subsequently updated to 1YEP) was subsequently depicted at 2.5 Å resolution, both in the FF and the LU states involved in different stages of peroxidase catalysis (Figures 1A and 1B) (Parsonage et al., 2005; Wood et al., 2002). In a follow-up, the structure of a *St*AhpC^{C46S} mutant was crystallized (PDB: 1N8J), revealing the resistance of bacterial PRDXs to hyperoxidation in comparison with eukaryotic 2-Cys PRDXs (Wood et al., 2003a, 2003b). Furthermore, two conserved motifs

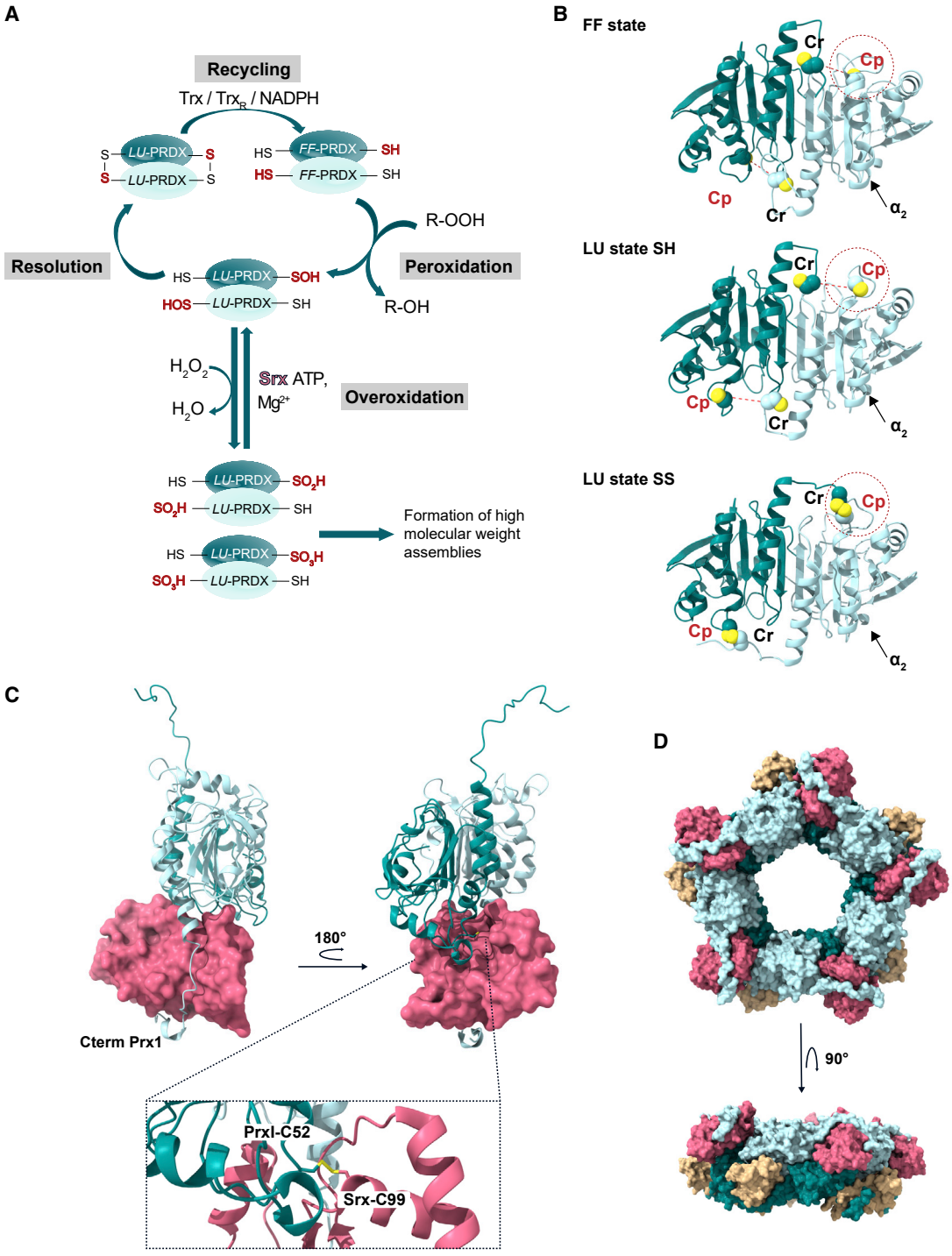

Figure 1. Structural details of the catalytic cycle of 2-Cys PRDXs

(A) Catalytic cycle of 2-Cys PRDXs. A peroxide molecule oxidizes Cys-S_P into Cys-S_POH. The sulfenic acid S_POH subsequently reacts with Cys-SH of another PRDX protomer forming a disulfide bond. Both subunits of PRDX contribute to the dimer assembly by providing either the C_P or the C_R to one of the active sites. This dimer can be reduced by the Trx/TrxR/NADPH system for regeneration. In eukaryotes, Cys-S_POH may easily react with another H_2O_2 molecule forming a sulfinic acid Cys-S_PO_2H resulting in the inactivation of peroxidase activity and the formation of HMW assemblies. This inactivation can be reversed by the Srx enzyme, or lead to the irreversible hyperoxidation to sulfonic acid Cys-C_PO_3H. Homodimers are colored in cyan and teal, respectively.

(B) AhpC in its FF state (PDB: 4XRD), LU-SH state (PDB: 4XS1) with local unfolding of α_2, and LU-SS state (PDB: 1YEP). The peroxidatic cysteine (C_P) and resolving cysteine (C_R) are labeled as well as the helix α_2, which transitions to a partially unfolded state enabling the formation of a disulfide between the two cysteine residues.

(C) Prx1-Srx complex (PDB: 2RII) with one sulfiredoxin molecule (pink surface) binding to a dimer of PrxI via a disulfide bond between Cys99 (Srx) and Cys52 (Prx1).

(D) Model of the structure of 10 Srx molecules (pink and light ochre) interacting with a 2-Cys PRDX decamer (homodimers in light blue and teal) (Jonsson et al., 2008). Figure reproduced and modified with permission from the authors and Nature Publishing Group (CC, 2021).

in eukaryotic PRDXs possibly responsible for their increased sensitivity to oxidation (GGLG and YF motifs) were identified (Wadley et al., 2016; Wood et al., 2003a, 2003b). Interestingly, a recent study on the yeast PRDX Tsa1 found the sensitivity to hyperoxidation not to be linked to the resolution step as expected, but to instead depend on the rates of two competing reactions: the structural transitions from the FF to the LU state as well as the oxidation to the sulfenic acid form (Kriznik et al., 2020).

In the *St*AhpC enzyme, Thr77Ile or Thr88Asp mutations disrupt the decameric assembly, whereas a Thr77Val mutant enhanced its stability (PDB: 1YF1, 1YEP, 1YF0, 1YEX). Subsequently, the effects of several point mutations located near the active site were evaluated by investigating the local structural re-arrangements imposed (PDB: 4XTS, 4XRA, 4XRD, 4XS1, 4XS4, 5UKA). This way, structural features of the FF state of AhpC, as well as the two distinct LU states (SH and S-S), could be discerned and correlated to catalytic efficiency (Figure 1B) (Nelson et al., 2018). As the hyperoxidized form of 2-Cys PRDXs exists as a stable decamer with the active site buried, it remained unclear how Srx could access the sulfinic acid moiety. The structural details of ATP-dependent binding to the human PrxI-Srx complex (PDB: 2RII) (Figure 1C) (Jonsson et al., 2005, 2008) revealed the complete unfolding of the PRDX C terminus and its unexpected packing onto the backside of Srx pointing away from the active site (Figure 1C) (Jonsson et al., 2008). Furthermore, modeling of the PrxI complex with ATP-bound Srx indicated that Asp187 of PrxI contacts Srx catalyzing ATP hydrolysis as well as the formation of a sulfinic acid phosphoryl ester. To understand how Srx interacts with the higher-order assemblies of PRDXs, a model of the decameric Prx1-Srx complex was generated (Figure 1D). The addition of ten Srx molecules expanded the toroid diameter (from ~110 to 125 Å) and thickness (from ~45 to 55 Å), suggesting that the binding of one or two Srx molecules to Prx1 decamers destabilizes PRDX-PRDX interactions in higher-order oligomers and thus effectively leads to their dissociation into dimers (Jonsson et al., 2008).

OVERVIEW OF STRUCTURAL INVESTIGATIONS ON HIGH-MOLECULAR-WEIGHT PRDXs SYSTEMS

In their seminal review from 2007 Karplus and Hall stated: "*Structural studies since the first peroxiredoxin structure was determined in 1998* (Choi et al., 1998)*, have produced 35 crystal structures of wild type and mutant peroxiredoxins with at least one representative structure from each of the five major evolutionary subfamilies of PRDXs*" (Karplus and Hall, 2007). The field has gained a remarkable momentum in the last two decades, as in 2020 the number of published crystal structures of PRDXs reached >3,000 PDB entries, reflecting the divergence and importance of this large class of proteins. Analyzing the available structures reveals that only about 3% (90) represent higher-order oligomeric species (decameric states or larger). These large molecular assemblies lie at the core of the PRDX chaperone function, indicating a general lack of available structural information for this important functional feature, especially in terms of chaperone-client interactions as so far only a single structure was reported with a bound client (Table 1).

The first crystal structure of a high-molecular-weight (HMW) 2-Cys PRDX, at 1.7 Å resolution, established that the third most abundant protein found in red blood cells, Prx2 (TPx-B [Moore et al., 1991]), adopts a decameric toroid structure (Schröder et al., 2000) (Figure 2A). The decamer is formed by five homodimers linked via weak hydrophobic interactions through the A type dimer-dimer interfaces where the monomers interact near their helix α_3 (Figure 2A) (Schröder et al., 1999, 2000). Following this pioneering study, a number of PRDXs from a variety of organisms have been studied using crystallography. In fact, a first study on Prx2 using negative stain EM data was published by Harris already in the 1960s (Harris, 1969). Despite the severely limited EM resolution at the time, the authors could still identify both ring-shaped decamers and stacked toroid-shaped rings of this PRDX system through transmission electron microscopy (TEM) and further characterization by crystallography (Harris, 1969; Harris et al., 2001).

For PRDXs from the archaea *Aeropyrum pernix K1* and *Pyrococcus horikoshii OT3*, numerous crystal structures of decameric states oxidized to different extents, in complex with a peroxide substrate or of mutant enzymes have been reported (Table 1) (Himiyama et al., 2019; Nakamura et al., 2006, 2008, 2010, 2013, 2017). In plants, lately two typical 2-Cys PRDXs, from *Chlamydomonas reinhardtii* and *Arabidopsis thaliana*, have been shown to preferentially exist in ring-shaped decameric forms, composed of pentamers of dimers (PDB: 6J13; 5ZTE) (Charoenwattanasatien et al., 2018; Yang et al., 2018).

STRUCTURAL DETERMINANTS OF PRDX OLIGOMERIZATION

Next, we first discuss structural determinants of PRDX oligomerization in two of the most well-studied systems to better prepare for the ensuing deliberation of structural determinants of chaperone activity (see oligomerization and dissociation of chaperone-active PRDXs below).

Prx2 from erythrocytes

Despite the fact that the Prx2 structure was originally characterized as a toroidal shaped protein, it was subsequently shown to exist in an equilibrium of decamers and dimers in solution (Harris, 1968; Schröder et al., 1999). The decameric state structure revealed the first insights into its three-dimensional ring-shaped assembly (Figure 2A) (Schröder et al., 2000). The peroxidatic cysteine Cys51 is in a hyperoxidized, sulfinic acid form, corresponding to an inactive FF state of the protein (PDB: 1QMV) (Figure 2A) since the second catalytic cysteine residue, Cys172, resides ~15 Å away from Cys51 and is unable to from the disulfide bond necessary for enzyme recycling (Figure 2A). Hyperoxidation of Cys51 allows the formation of a stable decamer, possibly further stabilized by a salt bridge between the sulfinic acid group of Cys51 and Arg127 (Figure 2A) (Wood et al., 2003a, 2003b). The oligomeric state of Prx2 was recently investigated in real time *in cellulo* using a technique based on the Förster resonance energy transfer (FRET) called homo-FRET (Pastor-Flores et al., 2020). Remarkably, a fusion protein of Prx2 and the fluorescent protein mCerulean exhibited polarization properties compatible with a mainly decameric assembly *in vivo*. Interestingly, complete dimerization of the enzyme

Table 1. Summary of the HMW PRDXs structures listed in the PDB

PDB ID	Reference	Peroxiredoxin system	Oligomeric state	Resolution (Å)
PDB: 6KHX	Li et al. (2020)	PRDX from *Akkermansia muciniphila*	homo-10-mer	2.58
PDB: 6J13	Charoenwattanasatien et al. (2020)	PRDX from *Chlamydomonas reinhardtii*	homo-10-mer	2.4
PDB: 6Q5V	Stroobants et al. (2019)	SiPRDX from *Sulfolobus islandicus*	homo-10-mer	2.7
PDB: 6ITZ	Himiyama et al. (2019)	PRDX from *Thermococcus kodakaraensis* and *Pyrococcus horikoshii*	homo-12-mer	2.96
PDB: 6IU0			homo-12-mer	2.38
PDB: 6IU1			homo-10-mer	2.89
PDB: 6E0F[a] PDB: 6E0G[a]	Teixeira et al. (2019)	mitochondrial PRDX from *Leishmania infantum* free and bound state with luciferase	homo-10-mer	3.7
PDB: 5OVQ	Liu et al. (2018)	AhpC2 from the hyperthermophilic bacteria *Aquifex aeolicus*	homo-12-mer	1.8
PDB: 5ZTE	Yang et al. (2018)	PrxAC119S from *Arabidopsis thaliana*	homo-10-mer	2.6
PDB: 5XBR	Nakamura et al. (2017)	peroxiredoxin from *Pyrococcus horikoshii*	homo-12-mer	2.1
PDB: 5IJT	Bolduc et al. (2018)	hPrx2 oxidized state	homo-10-mer	2.2
PDB: 5Y63	Pan et al. (2018)	EfAhpC from *Enterococcus faecalis*	homo-10-mer	2.9
PDB: 5JCG PDB: 5UCX		hPrx3 and hPrx3Ser78Cys as three stacked rings	homo-12-mer	2.4
PDB: 5B8A	Kamariah et al. (2016)	oxidized and reduced dimeric EcAhpC1-186-YFSKHN	homo-10-mer	2.7
PDB: 5B8B				3.1
PDB: 4L0U	Gretes and Karplus (2013)	Prx1a from *Plasmodium vivax*	homo-10-mer	2.5
PDB: 4XRD	Nelson et al. (2018)	StAhpC different mutants	homo-10-mer	2.3
PDB: 4XS1				2.1
PDB: 4XS4				2.7
PDB: 4XS6				3.4
PDB: 4XTS				2.7
PDB: 4XRA				1.8
PDB: 5DVB	Nielsen et al. (2016)	Tsa2 from *Saccharomyces cerevisiae* in the native state and the disulfide state	homo-10-mer	2.2
PDB: 5EPT				5.0
PDB: 4MH2	Cao et al. (2015)	oxidized and reduced forms of bovine mitochondrial Prx3	homo-12-mer	2.2
PDB: 4MH3				2.4
PDB: 4RQX	Parker et al. (2015)	hPrx4 with MESNA	homo-10-mer	2.3
PDB: 4O5R	Dip et al. (2014b)	AhpC from *E. coli*	homo-10-mer	3.3
PDB: 4QL7	Dip et al. (2014a)	C-terminal truncated AhpC1-172 and AhpC1-182 from *E. coli*	homo-10-mer	3.8
PDB: 4QL9				3.4
PDB: 4KB3	https://doi.org/10.2210/pdb4KB3/pdb	mitochondrial PRDX from *Leishmania braziliensis*	homo-10-mer	2.9
PDB: 4K1F	Brindisi et al. (2015)	tryparedoxin peroxidase I from *Leishmania major* LmTXNPx	homo-10-mer	2.3
PDB: 4MA9	Perkins et al. (2013)	StAhpC WT and StAhpCCys165Ala in their substrate-ready state	homo-10-mer	1.8
PDB: 4MAB				1.9
PDB: 4LLR	Pineyro et al. (2005)	tryparedoxin peroxidase from *Trypanosoma cruzi* in the reduced state	homo-10-mer	2.8
PDB: 3ZL5	Saccoccia et al. (2012)	SmPrxICys48Ser and SmPrxICys48Pro	homo-10-mer	2.49
PDB: 3ZLP				3.52
PDB: 3VWU	Sato et al. (2013)	Prx4 from *Mus musculus*	homo-10-mer	3.3
PDB: 4FH8	Nguyen et al. (2013)	Prx1 from *Ancylostoma ceylanicum* and the C-terminal truncated mutant bound to conoidin A	homo-10-mer	2.11
PDB: 4KW6				3
PDB: 3W6G	Nakamura et al. (2013)	PRDX from anaerobic hyperthermophilic archaeon *Pyrococcus horikoshii*	homo 20-mer	2.25
PDB: 3TUE	Fiorillo et al. (2012)	tryparedoxin Prx1 from *Leishmania major*	homo-10-mer	3

(*Continued on next page*)

Table 1. *Continued*

PDB ID	Reference	Peroxiredoxin system	Oligomeric state	Resolution (Å)
PDB: 3SBC	Tairum et al. (2012)	Tsa1Cys47Ser from *Saccharomyces cerevisiae*	homo-10-mer	2.8
PDB: 3ZVJ	Saccoccia et al. (2012)	LMW and HMW SmPrxI	homo-20-mer	3
PDB: 3ZTL			homo-10-mer	3
PDB: 3QPM	https://doi.org/10.2210/pdb3QPM/pdb	Prx4 from *Pseudosciaena crocea*	homo-10-mer	1.9
PDB: 3TJB	Cao et al. (2011)	hPrx4 WT, hPrx4Cys51Ala, and hPrx4Cys245Ala in different oxidation states	homo-10-mer	2.38
PDB: 3TJK				2.09
PDB: 3TJJ				1.91
PDB: 3TJG				2.24
PDB: 3TJF				2.04
PDB: 3TKP	Wang et al. (2012)	hPrx4 in different states and mutations	homo-10-mer	2.49
PDB: 3TKQ				2.22
PDB: 3TKR				2.1
PDB: 3TKS				2.4
PDB: 3A2V	Nakamura et al. (2010)	PRDXCys207Ser from *Aeropyrum pernix* K1 complexed with H_2O_2, acetate, and in reduced form	homo-10-mer	1.65
PDB: 3A2W				2.3
PDB: 3A2X				1.9
PDB: 3A5W				2.2
PDB: 3EMP	Nelson et al. (2008)	S-acetanilide modified form of StAhpCCys165Ser	homo-10-mer	4
PDB: 2ZCT	Nakamura et al. (2008)	PRDXCys207Ser from *Aeropyrum pernix* K1, oxidation, pre-oxidation, and sulfonic acid forms	homo-10-mer	1.7
PDB: 2E2G				2.4
PDB: 2E2M				2.6
PDB: 2NVL				2.36
PDB: 2Z9S	Matsumura et al. (2008)	rat HBP23/PRDXICys52Ser	homo-10-mer	2.9
PDB: 2PN8	https://doi.org/10.2210/pdb2PN8/pdb	hPrx4	homo-10-mer	1.8
PDB: 2H66	Vedadi et al. (2007), https://doi.org/10.2210/pdb2I81/pdb	PRDX from *Plasmodium vivax* native and reduced states	homo-10-mer	2.5
PDB: 2I81				
PDB: 1X0R	Nakamura et al. (2008)	thioredoxin peroxidase from *Aeropyrum pernix* K1	homo-10-mer	2
PDB: 1ZOF	Papinutto et al. (2005)	AhpC from *Helicobacter pylori*	homo-10-mer	2.95
PDB: 1ZYE	Cao et al. (2005)	bovine mitochondrial Prx3	homo-24-mer	3.3
PDB: 1YEP		StAhpC WT and 3 different mutants Thr77Ile, Thr77Asp, and Thr77Val	homo-10-mer	2.5
PDB: 1YEX				2.3
PDB: 1YF0				2.5
PDB: 1YF1				2.6
PDB: 2CV4	Mizohata et al. (2005)	archaeal peroxiredoxin from the aerobic hyperthermophilic crenarchaeon *Aeropyrum pernix* K1	homo-10-mer	2.3
PDB: 2BMX	Guimaraes et al. (2005)	AhpC from *Mycobacterium tuberculosis*	homo-12-mer	2.4
PDB: 1WE0	Kitano et al. (2005)	AhpC from *Amphibacillus xylanus*	homo-10-mer	2.9
PDB: 1N8J	Wood et al. (2003)	StAhpCCys46Ser	homo-10-mer	2.17
PDB: 1E2Y	Alphey et al. (2000)	tryparedoxin peroxidase from *Crithidia fasciculata*	homo-10-mer	3.2
PDB: 1QMV	Schroder et al. (2000)	thioredoxin peroxidase B (TPx-B) from red blood cells	homo-10-mer	1.7

[a]Structure solved by single-particle EM.

upon H_2O_2 addition was accompanied by only partial disulfide bond formation, suggesting that intermolecular disulfide bond formation in one or two dimers within the decamer is sufficient to trigger complete decamer dissociation into dimers. Upon elevated H_2O_2 levels and hyperoxidation, shifts in fluorescence polarization support decamer stacking (Pastor-Flores et al., 2020). Based on negative stained TEM images a "cage" structure dodecahedron of human Prx2 consisting of 12 decamers

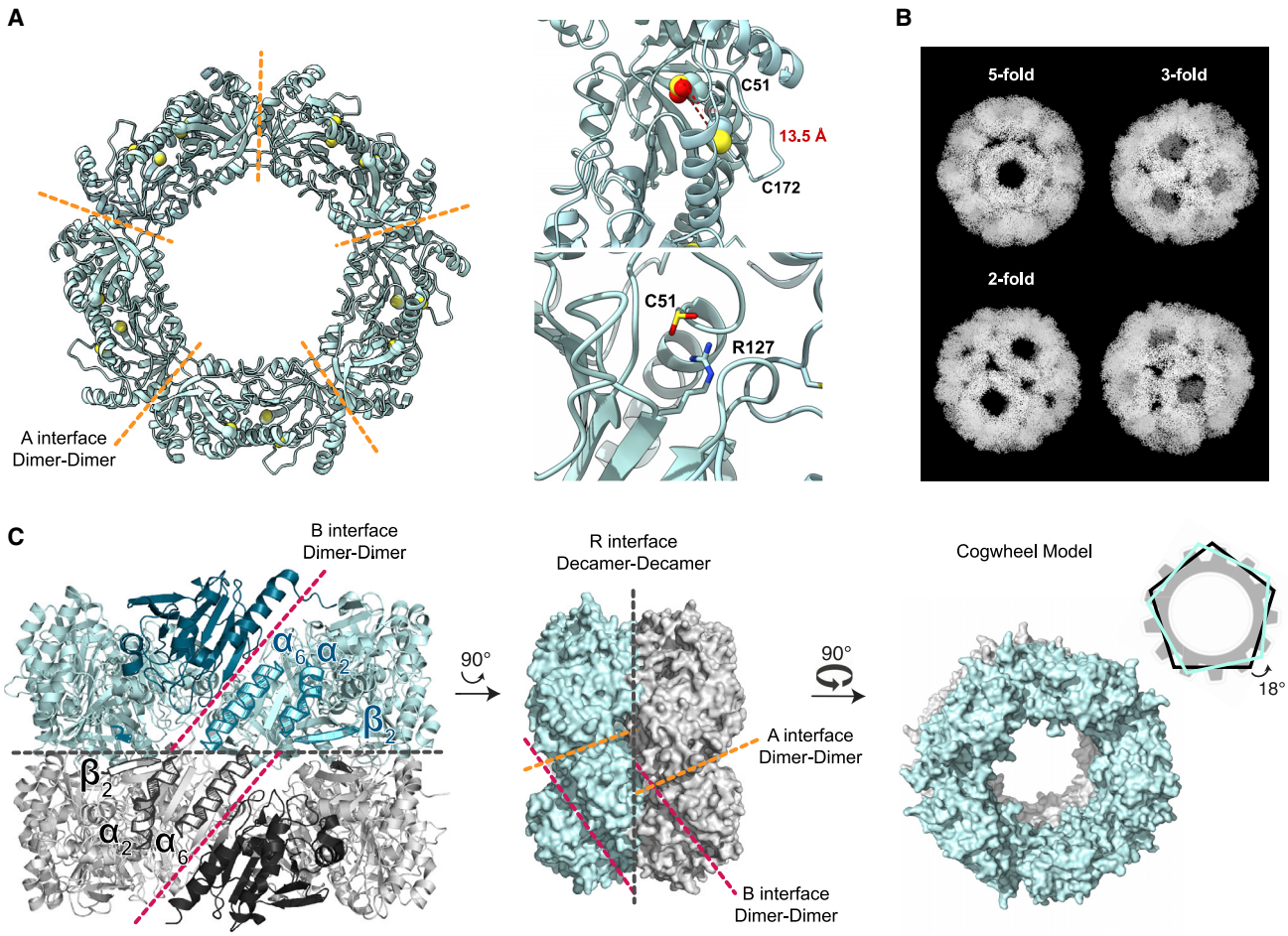

Figure 2. Structural features of 2-Cys Prx oligomer HMW assemblies

(A) Visualization of the toroidal decamer of Prx2 solved by X-ray crystallography, with a particular focus on the distance between the hyperoxidized peroxidatic Cys51 (C_P-SO_2H) and the resolving Cys172, as well as the Cys51-Arg127 interaction (right panels). The dimer-dimer A interfaces are indicated by the broken line (orange). Cysteine residues are shown as spheres and colored according to heteroatoms (PDB: 1QMV).

(B) Reconstructed images of the PRDX dodecahedron assembly in its "cage" structure obtained from single-particle TEM micrographs with a medium resolution of 16 Å, with 2-, 3-, and 5-fold symmetry axes. Images produced by U. Meissner and kindly provided by J.R. Harris (Meissner et al., 2007).

(C) The cogwheel ring model adopted by the 2-Cys PRDX *Sm*PRX1. Visualization of the different interfaces formed between the stacked decamers (R interface, black) and homodimers (A and B interfaces in orange and magenta). α_2 and α_6 helices create a negatively charged patch interacting with positively charged residues on the opposing interface to stabilize the double decameric architecture forming the R interface. The cogwheel architecture derives from the interaction of β_2 strands of two opposing subunits by additional polar contacts surrounding this interface. Monomer units are colored in black and dark cyan in the two decameric rings, respectively. Helices α_2 and α_6, as well as the β_2 strand, are outlined within the structure. Rotations between individual views and the 18° twist of the assembled two decameric rings are indicated. Figure adapted and extended from Saccoccia et al. (2012) (PDB: 3ZVJ) with permission (CC, 2021).

could be assembled *in vitro* (Meissner et al., 2007) (Figure 2B). Importantly, even though *in vivo* confirmation of the existence of this HMW structure still remains elusive, hyperoxidation has been noted to foster the formation of stable and compact decameric species (Perkins et al., 2015).

*Hs*Prx3

The structural determinants underlying multimerization of the human mitochondrial 2-Cys *Hs*Prx3, which under acidic conditions is decoupled from its redox state, were studied using cryoelectron microscopy (cryo-EM) (PDB: toroidal oligomers 5JCG, filaments 5UCX). The first high-resolution structure of this protein by single-particle analysis of TEM images and under acidic conditions (pH 4) revealed dodecameric assemblies in the form of long, highly ordered nanotubes (Phillips et al., 2014). The stacking of the individual dodecamers depended on hydrogen bonds between the α_2/α_6 helices, as well as the β_2 strand (see the corresponding structural features within *Sm*PrxI in Figure 2C). Furthermore, the C terminus was suggested to control the switch between peroxidase and holdase activity, a feature initially proposed by Saccoccia et al. (2012) for *Sm*PrxI. In *Hs*Prx3, the partially folded C terminus provides an additional hydrophobic surface, enabling the stacking of individual dodecamers, whereas for *Sm*PrxI the C terminus seems to be unfolded allowing the decamer-decamer interaction (Radjainia et al., 2015; Saccoccia et al., 2012). The correlation between the distribution of hydrophobic surfaces of different model HMW PRDXs and increased holdase function, suggests that exposed hydrophobic surfaces play an important role in their chaperone activities (Angelucci et al., 2013; Radjainia et al., 2015). In *Hs*Prx3 HMW helical filaments were detected at

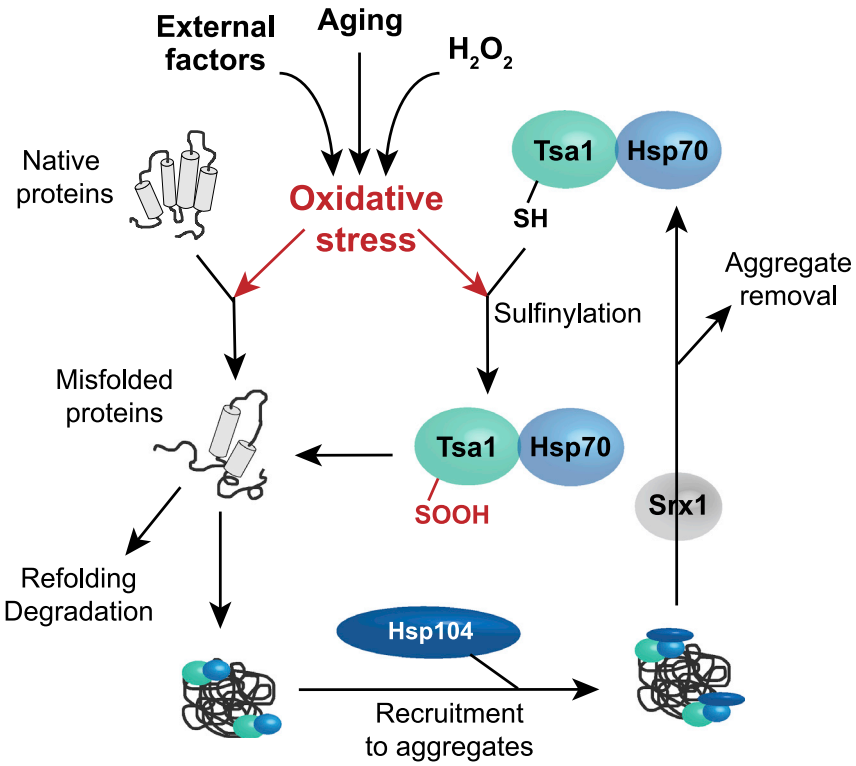

Figure 3. Proposed chaperone network of Tsa1

Sequential recruitment of the peroxiredoxin Tsa1 and the chaperones Hsp70 and Hsp104 to misfolded proteins followed by Tsa1 dissociation, which is triggered by the ATP-dependent peroxiredoxin sulfinic acid reductase Srx1 to allow aggregate resolution. Adapted and modified from Hanzen et al. (2016), with permission from the authors and the Elsevier publishing group.

both pH 4.0 and pH 8.5. The active site adopted two distinct conformations, an LU state under acidic conditions and an FF state under basic conditions, suggesting that *Hs*Prx3 HMW maintains catalytic activity in the filamentous structure. The main differences between both states lies in the structure of the C terminus, being in an FF state under basic conditions, whereas an LU state dominates at low pH, enabling additional electrostatic interactions at the R interface. The clustering of *Hs*Prx3 was hypothesized to constitute proof of its self-associating chaperone activity, providing a protective mechanism against protein aggregation in the crowded mitochondrial environment.

OLIGOMERIZATION AND DISSOCIATION OF CHAPERONE-ACTIVE PRDXs

In this section we discuss molecular determinants of PRDX chaperone function in the three best-understood examples so far, namely Tsa1 from *S. cerevisiae*, PrxI from *S. mansoni*, and mTXNP from *L. infantum*.

S. cerevisiae Tsa1

The ability of 2-Cys PRDXs to inhibit protein aggregation *in vitro* was initially described for the *S. cerevisiae* Tsa1 enzyme (Jang et al., 2004). Notably, expression of Tsa1 in a deletion strain lacking both Tsa1/Tsa2 also improved the ability of cells to survive heat shock (Jang et al., 2004). Furthermore, either the hyperoxidation of the catalytic cysteine or heat shock acting independently of enzyme oxidation, resulted in a reversible structural switch of Tsa1 from low-molecular-weight (LMW) to HMW complexes *in vivo* (Jang et al., 2004). The inherent chaperone activity correlated directly with two factors: enzyme multimerization and the exposure of hydrophobic segments (Jang et al., 2004; Nielsen et al., 2016; Tairum et al., 2012, 2016). Tsa1 multimerization upon H_2O_2 addition is linked to the degree of enzyme sulfinylation (Jang et al., 2004) and *in vivo* chaperone-active Tsa1 attains a size compatible with double decamerization (Noichri et al., 2015). Also irreversible oxidation of the C_P to SO_3H leads to multimerization into double decameric ring structures and stimulated Tsa1 chaperone activity (Lim et al., 2008). Evidence that chaperone-active Tsa1 interacts with other molecular chaperones *in vivo* comes from the observation that the main cytosolic Hsp70 molecular chaperones (Ssa1/2 in *S. cerevisiae*) require Tsa1 to bind to aggregates both in aged cells and upon H_2O_2 addition (Figure 3) (Hanzen et al., 2016). The recruitment of Hsp70 requires Tsa1 hyperoxidation and correlates with the formation of HMW assemblies (Noichri et al., 2015). Remarkably, efficient *in vivo* aggregate resolution requires both Tsa1 sulfinic acid reduction by Srx1, as well as interplay with Hsp70 and the disaggregase Hsp104, in a sequential manner (Figure 3) (Hanzen et al., 2016). Interestingly, the key role of Srx1 in resolving H_2O_2-induced aggregates appears to be accompanied by inactivation of one of the main cytosolic Hsp40s, Ydj1, a type I zinc finger containing Hsp40 (Brandes et al., 2011; Choi et al., 2006; Hanzen et al., 2016), but not the type II Hsp40 Sis1 lacking the cysteine-containing zinc finger domain (Hanzen et al., 2016). In contrast, Ydj1 is absolutely essential for the resolution of aggregates formed upon heat shock.

Furthermore, the key role of Tsa1 in Hsp70/Hsp104 substrate binding upon H_2O_2 addition seems distinct from the roles of certain sHsps. The *S. cerevisiae* sHsp Hsp26 has been proposed to maintain small-size aggregates, thus providing increased substrate accessibility for Hsp70, but also to partially compete with Hsp70 for substrate binding (Zwirowski et al., 2017). In this regard, the *in vivo* Tsa1 chaperone function upon H_2O_2 stress resembles that of cellular aggregate sorting factors, such as the sHsp Hsp42, in facilitating the formation of distinctly localized cellular protein inclusions that were proposed to counteract Hsp70 overload upon proteostatic dysfunction (Ho et al., 2019). However, Hsp42 inclusions formed independently of Tsa1 upon H_2O_2 addition (Hanzen et al., 2016), suggesting that the proteins perform independent functions in protein quality control under these conditions.

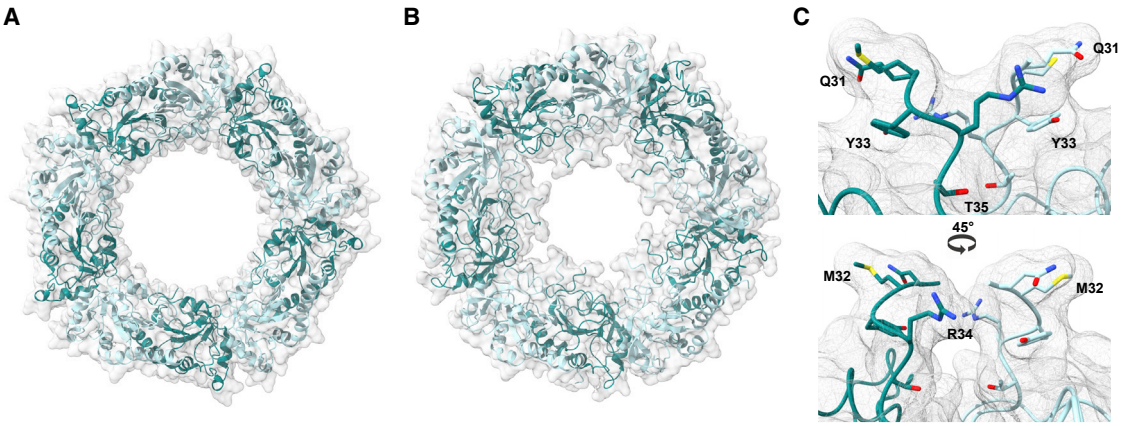

Figure 4. Cryo-EM structures of decameric mTXNPx from *Leishmania infantum*
The structures of mTXNPx in its free (A) and bound state (B) obtained, respectively, with 2.9 and 3.7 Å resolution with luciferase as the client protein (PDB: free mTXNPx 6E0G, luciferase bound mTXNPx 6E0F). N-Terminal residues Gln31-Thr35 shown docked into the mTXNPx$_{red}$:luciferase map extending to form an inner ring distinct from the larger decamer structure (C). Adapted from Teixeira et al., (2019) with permission from the authors and Nature Publishing Group (CC, 2021).

S. mansoni PrxI

The human parasite *Schistosoma mansoni* expresses a single 2-Cys PRDX that, upon hyperoxidation by H_2O_2, as well as under acidic conditions, forms double decameric structures (Table 1, PDB: HMW state 3ZVJ; LMW state 3ZTL) (Saccoccia et al., 2012). Under acidic conditions (pH 4.2) chaperone-active *Sm*PrxI almost completely oligomerizes into double decamers (Saccoccia et al., 2012). Comparison with the reduced enzyme reveals that the α_2/α_6 helices facilitate decameric stacking, creating an interface between the two rings (the R interface), whereas the contacts between β_2 strands of two opposing subunits surrounding this interface leads to a characteristic cogwheel architecture (Figure 2C).

The enzyme interacts with citrate synthase through hydrophobic patches exposed upon unfolding of the C terminus and the α_2 helix, bearing the peroxidatic cysteine, in one of the two decamers. Mutants destabilizing helix α_2 and thus increasing the exposure of the active site hydrophobic patch (either lacking the C terminus or Cys48Pro/Cys48Asp substitutions) showed increased holdase activity. Similarly, hyperoxidation into SO_2H/SO_3H increased chaperone activity, correlating with the destabilization and partial unwinding of the α_2 helix (Saccoccia et al., 2012). Low pH, hyperoxidation, and high protein concentrations induced the formation of an HMW state of *Sm*PrxI exhibiting enhanced holdase activity. However, an *Sm*PrxI^{Cys48Ser} mutant constitutively assembling into double decamers is almost completely devoid of chaperone activity (Angelucci et al., 2013), suggesting that double decamerization is not sufficient for this activity. Instead, the ability to undergo conformational changes appears to be mandatory for holdase activity. This hypothesis is further supported by the observation that hyperoxidized *Sm*PrxI, which elutes as a mixture of different conformers, including double decamers and lower-molecular-weight assemblies upon size-exclusion chromatography, exhibits increased chaperone activity compared with the enzyme under acidic conditions, upon which the enzyme almost exclusively assembles into double decamer structures.

L. infantum mTXNP

The mammalian parasite *Leishmania infantum* expresses a typical 2-Cys PRDX within its mitochondria, mTXNP, that has been shown to be essential for virulence (Castro et al., 2011). This enzyme shares with other 2-Cys PRDXs the pentamer of dimers overall architecture, but appears to exhibit a chaperone activity restricted to its decameric, reduced form Teixeira et al. (2015, 2019). In contrast, in its dimeric, oxidized state, mTXNP neither inhibits aggregation nor is capable of maintaining client proteins in a folding-competent state (Castro et al., 2011; Teixeira et al., 2015). Furthermore, the expression of mTXNP in an *E. coli* chaperone-deficient *rpoH* mutant strain reduced protein aggregation, in agreement with the enzyme exhibiting an inherent chaperone function *in vivo*. EM-negative stain micrographs indicate that unfolded luciferase binds mTXNP within the center of its decameric ring (Figures 4A and 4B; Table 1) in a manner reminiscent of substrate encapsulation by chaperonins, such as GroEL. Subsequently, single-particle cryo-EM revealed contacts between the flexible N terminus of mTXNP, forming an inner ring, and unfolded luciferase (Figures 4B and 4C). *In vitro* and *in vivo* crosslinking experiments of recombinantly expressed mTXNP indicated additional residues at the dimer-dimer interface contacting the unfolded luciferase. Intriguingly, several of these residues are normally buried within the structure, and therefore not directly accessible to client proteins, indicating structural re-arrangements within the dimer-dimer interface. Therefore, dissociation might destabilize the hydrophobic dimer-dimer interface facilitating the exposure of binding sites for unfolded client proteins, in agreement with crosslinking experiments that supported enzyme dissociation into dimers upon heat shock (Teixeira et al., 2019). This behavior is strongly reminiscent of sHsps and J-domain-independent holdase activities of Hsp40 chaperones, which are the focus of the next section.

SMALL HSPs AND J-DOMAIN-INDEPENDENT HSP40 HOLDASES AS BLUEPRINTS FOR THE PRDX CHAPERONE FUNCTION

Small HSPs

sHSPs are ATP-independent chaperones existing in a range of dynamic ensembles of different oligomeric species

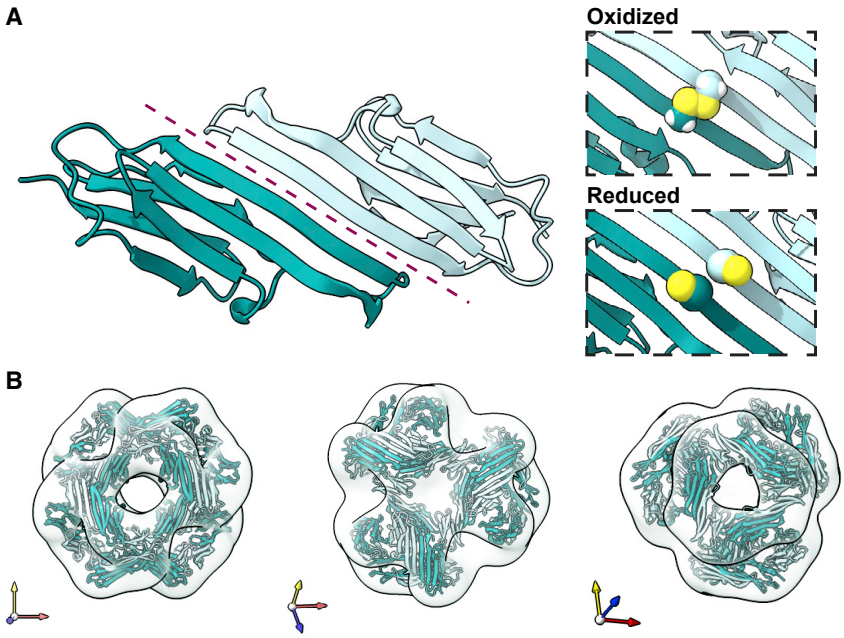

Figure 5. Hsp27 dimeric and higher-order oligomeric structural arrangements

Visualization of the core domain of dimeric Hsp27 and the formation of the inter-dimer disulfide bond occurring at the β sheet interface (visible in red) between residues Cys137 during oxidation of the chaperone (A), and its suggested structural arrangement into a globular 24-mer assembly during its thermally induced self-association, as observed for human αB-crystallin (fit into EM map, EMD-1776) (B). In the structural model, the 24-mer possesses a central cavity, surrounded by flexible N-terminal residues. The empty central cavity visible here on the EM map may be due to missing electron density.

(Haley et al., 2000; Haslbeck et al., 2019; Jakob et al., 1993). From their LMW monomeric state, ranging from 12 to 43 kDa, these proteins can assemble into large supramolecular assemblies up to 400 kDa, in the form of highly ordered spherical cage-like structures (Mogk et al., 2019; White et al., 2006). Functionally, they can be characterized as holdase chaperones, as they are devoid of ATP-driven refolding functions (Haslbeck et al., 2019). Several sHSPs (αB-crystallin, Hsp26, Hsp27, Hsp22, and HspB2) exhibit temperature-dependent chaperone properties by preventing the aggregation of distinct target proteins (Bakthisaran et al., 2015). For instance, *S. cerevisiae* Hsp26 forms an inactive 24-mer complex at normal temperature that, upon heat shock, dissociates into chaperone-active dimeric structures (Haslbeck et al., 1999). Upon unfolding, Hsp26 exposes hydrophobic regions that are thought to bind non-native client proteins. Intriguingly, a cryo-EM study of Hsp26 revealed two distinct populations—a compact and an extended state—consisting of 24 subunits arranged in a porous shell with tetrahedral symmetry, reminiscent of the reconstructions of dodecahedrons for Prx2 (Meissner et al., 2007; White et al., 2006). PRDXs have also been proposed to unfold upon chaperone activation, although not to a similar extent (Voth and Jakob, 2017). On the contrary, Hsp27 undergoes thermally induced self-association, leading to oligomerization of the protein, correlating with an enhanced chaperone activity (Lelj-Garolla and Mauk, 2006). Finally, HspB2 transitions into a molten globule-like state at increased temperature, with a compact core formed of stable secondary structure elements but a partially unfolded tertiary structure, coupled to increased chaperone-like activity (Prabhu et al., 2012). Earlier studies indicated that the chaperone activity of sHSPs can be improved by using low concentrations of denaturing chaotropic agents (urea, GdHCl) inducing a molten globule state (Das and Liang, 1997; Raman and Rao, 1994).

Structurally, sHSPs are composed of disordered termini as well as an approximately 100-residue so-called α-crystallin domain, a highly conserved feature shared by all sHSPs (Jehle et al., 2009) (Figure 5). Shortly after the major α-crystallin protein reported in 1992 (Horwitz, 1992), bovine αB-crystallin and murine Hsp25 were also reported to exhibit chaperone activity (Jakob et al., 1993). Later, the isolated α-crystallin domain of αB-crystallin was shown to retain full chaperone activity *in vitro* (Jehle et al., 2009). However, more recent evidence pin point the importance of all three different sHsp domains in chaperoning different substrates (Haslbeck and Vierling, 2015; Mainz et al., 2015). Crystallography and solid-state NMR studies demonstrated that the αB-crystallin core readily dimerizes, forming a central antiparallel β sheet, a building block for the subsequent formation of higher-order oligomers, both features reminiscent of the typical 2-Cys PRDXs (Figure 5A) (Baldwin et al., 2012). A combination of techniques helped elucidate a symmetrical 24-mer oligomer structure of αB-crystallin (Figure 5B) (Jehle et al., 2011; Peschek et al., 2009). Different parts of the αB-crystallin protein are responsible for its multimerization, with the N-terminal domain facilitating the higher-order assembly, similar to mTXNP employing its unfolded N terminus for client binding within the central inner cavity (Chuang et al., 2006), whereas the *Sm*PrxI C terminus stabilizes decamer-decamer stacking (Angelucci et al., 2013; Saccoccia et al., 2012; Teixeira et al., 2019). Despite its polydispersity and inherent dynamics, a detailed understanding of how molecular motions govern αB-crystallin oligomeric distribution and, therefore, its function has been achieved (reviewed in Delbecq and Klevit, 2013; Hochberg and Benesch, 2014).

Hsp27 exhibits a redox-linked functional switch linked to partial unfolding of the α-crystallin domain inducing increased dynamics at the dimer interface (Figure 5A) (Alderson et al., 2019). Whereas Hsp27 easily assembles into oligomers, monomers formed upon reduction have been found to enhance chaperone activity *in vitro*, a feature coupled to an increased self-aggregation propensity (Alderson et al., 2019). Remarkably, the reduction of double decameric chaperone-active hyperoxidized Tsa1 by the ATP-dependent Srx1 into dimers was shown to be necessary for efficient *in vivo* aggregate resolution (Hanzen et al., 2016; Noichri et al., 2015), pointing to further structural and functional similarities between PRDXs and sHSPs.

Conversely, the peroxidatic cysteine-substituted Tsa1^{Cys48Ser} and the C-terminally truncated, sulfinylation-deficient Tsa1$^{\Delta YF}$, constitutively assembled into the double decamer form while remaining chaperone inactive (Noichri et al., 2015). This suggests that the ability to switch between LMW and HMW forms is crucial for *in vivo* Tsa1 chaperone activity.

However, whereas the ability of Hsp27 to disperse into free monomers and its chaperone activity were linked to the reduction of disulfide-linked monomers, the dissociation of Tsa1 double decamers appears to be linked to enzyme desulfinylation. If the former is presumably linked to the action of thioredoxins, the latter is ATP dependent and involves the reduction of the sulfinylated double decamer by Srx1.

Taken together, the monomerization of the molecular chaperone Hsp27, therefore also its function, is regulated by redox state in a remarkably similar manner, as described for PRDXs, through an inter-dimer disulfide bond. Notably, Hsp27 chaperone function correlates with an increase in the local concentration of free monomers. The situation is less clear for the PRDXs, with most of the characterized enzymes showing an enhanced chaperone activity upon multimerization into HMW assemblies, whereas other PRDXs rely on dissociation of oligomeric forms into dimers (Hanzen et al., 2016; Noichri et al., 2015; Teixeira et al., 2015).

J-domain-independent Hsp40 holdases

It is becoming increasingly clear that several J-proteins, both of the zinc finger domain containing (class I) and lacking (class II) types, also carry out J-domain-independent chaperone functions (Ajit Tamadaddi and Sahi, 2016; Craig and Marszalek, 2017). Of the former, the yeast class I J-protein and general Hsp70 co-chaperone, Ydj1, has been known for quite some time to inhibit rhodanese aggregation independently of the J-domain through a holdase-like activity (Jiang et al., 2019; Lu and Cyr, 1998). Of the class II Hsp40s, the human DnaJB6b has attracted special attention due to its potent, J-domain-independent ability to suppress amyloid aggregate formation *in vivo* and *in vitro* (Gillis et al., 2013; Mansson et al., 2014a, 2014b). Many J-proteins assemble into homodimeric structures (Craig and Marszalek, 2017; Soderberg et al., 2018). However, recent structural and functional studies of DnaJB6b and of its isolated C-terminal substrate-binding and oligomerization domain support a polydisperse structural arrangement into monomers, dimers, and oligomers ($\leq$40-mers) and a key role of a serine- and threonine-rich domain immediately preceding the C terminus in its interactions with substrate, in controlling reversible oligomerization as well as in the inhibition of amyloid-β aggregation (Karamanos et al., 2020; Soderberg et al., 2018). Different Hsp40s seem to employ slightly dissimilar modes of substrate interaction (Jiang et al., 2019) and much is still to learn regarding the structural determinants of the J-domain-independent holdase activities of the Hsp40s. Nevertheless, the fact that the DnaJB6b example showcases another Hsp70-coupled, ATP-independent chaperone mechanism resembling that employed by the PRDXs, underscores the importance of dynamic oligomerization and dissociation in chaperone holdase function and pinpoints the need to clarify the roles of PRDX dimers, and potentially monomers, in peroxiredoxin chaperone function. Future detailed studies are certainly warranted to improve our understanding of molecular and structural determinants exhibited by the chaperone activity of the enigmatic peroxiredoxins.

OUTLOOK

The recent revolution in single-particle cryo-EM has already provided novel opportunities for in-depth structural characterization of HMW PRDXs. Through solving the entire structure of supramolecular biological entities directly in their native environment, unprecedented details on their conformation and orientation were acquired, as recently pioneered by Teixeira et al., (2019) on the mTXNP peroxiredoxin system, and several other studies on related HMW peroxiredoxin assemblies. Since structures are determined under conditions closer to physiology than those solved by X-ray crystallography, cryo-EM also holds great promise for applications in structure-based drug design.

Following the initial characterization of the functional switches linked to the chaperone activity of PRDXs, we can expect further crucial insight related to interactions with different substrates in the near future illuminating their role as molecular chaperones. The latest improvements in NMR techniques may be expected to pave the way for structural and especially dynamical studies of such HMW complexes at atomic resolution in the way that NMR spectroscopy has lately driven the progress in the understanding of chaperone-client complexes.

ACKNOWLEDGMENTS

The authors are indebted to W.T. Lowther, U. Jakob, and J.R. Harris for sharing data aiding the production of the structural images presented, to the Swedish NMR Centre of the University of Gothenburg for providing an excellent research infrastructure, and to Michel B. Toledano for providing valuable comments on the manuscript. M.M. is thankful for funding from the Wallenberg Center for Molecular and Translational Medicine, University of Gothenburg, Cancerfonden, and the Swedish Research Council. B.M.B. gratefully acknowledges funding from the Swedish Research Council and the Knut och Alice Wallenberg Foundation through a Wallenberg Academy Fellowship as well as through the Wallenberg Centre for Molecular and Translational Medicine, University of Gothenburg.

AUTHOR CONTRIBUTIONS

Conceptualization, M.M. and L.T.; funding acquisition, M.M. and B.M.B.; visualization, L.T.; writing – original draft, L.T., B.M.B., and M.M.; writing – review & editing, M.M., B.M.B., and L.T.

DECLARATION OF INTERESTS

The authors declare no competing interests.

REFERENCES

Ajit Tamadaddi, C., and Sahi, C. (2016). J domain independent functions of J proteins. Cell Stress Chaperones *21*, 563–570.

Alderson, T.R., Roche, J., Gastall, H.Y., Dias, D.M., Pritisanac, I., Ying, J., Bax, A., Benesch, J.L.P., and Baldwin, A.J. (2019). Local unfolding of the HSP27 monomer regulates chaperone activity. Nat. Commun. *10*, 1068.

Alphey, M.S., Bond, C.S., Tetaud, E., Fairlamb, A.H., and Hunter, W.N. (2000). The structure of reduced tryparedoxin peroxidase reveals a decamer and insight into reactivity of 2Cys-peroxiredoxins. J. Mol. Biol. *300*, 903–916.

Anfinsen, C.B. (1973). Principles that govern the folding of protein chains. Science *181*, 223–230.

Angelucci, F., Saccoccia, F., Ardini, M., Boumis, G., Brunori, M., Di Leandro, L., Ippoliti, R., Miele, A.E., Natoli, G., Scotti, S., et al. (2013). Switching between the alternative structures and functions of a 2-Cys peroxiredoxin, by site-directed mutagenesis. J. Mol. Biol. *425*, 4556–4568.

Bakthisaran, R., Tangirala, R., and Rao Ch, M. (2015). Small heat shock proteins: role in cellular functions and pathology. Biochim. Biophys. Acta *1854*, 291–319.

Balchin, D., Hayer-Hartl, M., and Hartl, F.U. (2016). *In vivo* aspects of protein folding and quality control. Science *353*, aac4354.

Baldwin, A.J., Walsh, P., Hansen, D.F., Hilton, G.R., Benesch, J.L., Sharpe, S., and Kay, L.E. (2012). Probing dynamic conformations of the high-molecular-weight αβ-crystallin heat shock protein ensemble by NMR spectroscopy. J. Am. Chem. Soc. *134*, 15343–15350.

Barranco-Medina, S., Lazaro, J.J., and Dietz, K.J. (2009). The oligomeric conformation of peroxiredoxins links redox state to function. FEBS Lett. *583*, 1809–1816.

Biteau, B. (2003). ATP-dependent reduction of cysteine-sulphinic acid by *S. cerevisiae* sulphiredoxin. Nature *425*, 980–984.

Bodvard, K., Peeters, K., Roger, F., Romanov, N., Igbaria, A., Welkenhuysen, N., Palais, G., Reiter, W., Toledano, M.B., Kall, M., et al. (2017). Light-sensing via hydrogen peroxide and a peroxiredoxin. Nat. Commun. *8*, 14791.

Bolduc, J.A., Nelson, K.J., Haynes, A.C., Lee, J., Reisz, J.A., Graff, A.H., Clodfelter, J.E., Parsonage, D., Poole, L.B., Furdui, C.M., et al. (2018). Novel hyperoxidation resistance motifs in 2-Cys peroxiredoxins. J. Biol. Chem. *293*, 11901–11912.

Brandes, N., Reichmann, D., Tienson, H., Leichert, L.I., and Jakob, U. (2011). Using quantitative redox proteomics to dissect the yeast redoxome. J. Biol. Chem. *286*, 41893–41903.

Brindisi, M., Brogi, S., Relitti, N., Vallone, A., Butini, S., Gemma, S., Novellino, E., Colotti, G., Angiulli, G., Di Chiaro, F., et al. (2015). Structure-based discovery of the first non-covalent inhibitors of *Leishmania major* tryparedoxin peroxidase by high throughput docking. Sci. Rep. *5*, 9705.

Burmann, B.M., and Hiller, S. (2015). Chaperones and chaperone-substrate complexes: dynamic playgrounds for NMR spectroscopists. Prog. Nucl. Magn. Reson. Spectrosc. *86-87*, 41–64.

Burmann, B.M., Wang, C., and Hiller, S. (2013). Conformation and dynamics of the periplasmic membrane-protein-chaperone complexes OmpX-Skp and tOmpA-Skp. Nat. Struct. Mol. Biol. *20*, 1265–1272.

Cao, Z., McGow, D.P., Shepherd, C., and Lindsay, J.G. (2015). Improved catenated structures of bovine peroxiredoxin III F190L reveal details of ring-ring interactions and a novel conformational state. PLoS One *10*, e0123303.

Cao, Z., Roszak, A.W., Gourlay, L.J., Lindsay, J.G., and Isaacs, N.W. (2005). Bovine mitochondrial peroxiredoxin III forms a two-ring catenane. Structure *13*, 1661–1664.

Cao, Z., Tavender, T.J., Roszak, A.W., Cogdell, R.J., and Bulleid, N.J. (2011). Crystal structure of reduced and of oxidized peroxiredoxin IV enzyme reveals a stable oxidized decamer and a non-disulfide-bonded intermediate in the catalytic cycle. J. Biol. Chem. *286*, 42257–42266.

Castro, H., Teixeira, F., Romao, S., Santos, M., Cruz, T., Florido, M., Appelberg, R., Oliveira, P., Ferreira-da-Silva, F., and Tomas, A.M. (2011). *Leishmania* mitochondrial peroxiredoxin plays a crucial peroxidase-unrelated role during infection: insight into its novel chaperone activity. Plos Pathog. *7*, e1002325.

CC. (2021). Attribution 4.0 international. https://creativecommons.org/licenses/by/4.0/, Creative Commons.

Chae, H.Z., Chung, S.J., and Rhee, S.G. (1994). Thioredoxin-dependent peroxide reductase from yeast. J. Biol. Chem. *269*, 27670–27678.

Charoenwattanasatien, R., Tanaka, H., Zinzius, K., Hochmal, A.K., Mutoh, R., Yamamoto, D., Hippler, M., and Kurisu, G. (2018). X-ray crystallographic and high-speed AFM studies of peroxiredoxin 1 from *Chlamydomonas reinhardtii*. Acta Crystallogr. *74*, 86–91.

Charoenwattanasatien, R., Zinzius, K., Scholz, M., Wicke, S., Tanaka, H., Brandenburg, J.S., Marchetti, G.M., Ikegami, T., Matsumoto, T., Oda, T., et al. (2020). Calcium sensing via EF-hand 4 enables thioredoxin activity in the sensor-responder protein calredoxin in the green alga *Chlamydomonas reinhardtii*. J. Biol. Chem. *295*, 170–180.

Cho, C.S., Lee, S., Lee, G.T., Woo, H.A., Choi, E.J., and Rhee, S.G. (2010). Irreversible inactivation of glutathione peroxidase 1 and reversible inactivation of peroxiredoxin II by H_2O_2 in red blood cells. Antioxid. Redox Signal. *12*, 1235–1246.

Choi, H.I., Lee, S.P., Kim, K.S., Hwang, C.Y., Lee, Y.R., Chae, S.K., Kim, Y.S., Chae, H.Z., and Kwon, K.S. (2006). Redox-regulated cochaperone activity of the human DnaJ homolog Hdj2. Free Radic. Biol. Med. *40*, 651–659.

Choi, H.J., Kang, S.W., Yang, C.H., Rhee, S.G., and Ryu, S.E. (1998). Crystal structure of a novel human peroxidase enzyme at 2.0 Å resolution. Nat. Struct. Biol. *5*, 400–406.

Chuang, M.H., Wu, M.S., Lo, W.L., Lin, J.T., Wong, C.H., and Chiou, S.H. (2006). The antioxidant protein alkylhydroperoxide reductase of *Helicobacter pylori* switches from a peroxide reductase to a molecular chaperone function. Proc. Natl. Acad. Sci. U S A *103*, 2552–2557.

Craig, E.A., and Marszalek, J. (2017). How do J-proteins get Hsp70 to do so many different things? Trends Biochem. Sci. *42*, 355–368.

Das, B.K., and Liang, J.J. (1997). Detection and characterization of α-crystallin intermediate with maximal chaperone-like activity. Biochem. Biophys. Res. Commun. *236*, 370–374.

Delbecq, S.P., and Klevit, R.E. (2013). One size does not fit all: the oligomeric states of αB crystallin. FEBS Lett. *587*, 1073–1080.

Dip, P.V., Kamariah, N., Nartey, W., Beushausen, C., Kostyuchenko, V.A., Ng, T.S., Lok, S.M., Saw, W.G., Eisenhaber, F., Eisenhaber, B., et al. (2014a). Key roles of the *Escherichia coli* AhpC C-terminus in assembly and catalysis of alkylhydroperoxide reductase, an enzyme essential for the alleviation of oxidative stress. Biochim. Biophys. Acta *1837*, 1932–1943.

Dip, P.V., Kamariah, N., Subramanian Manimekalai, M.S., Nartey, W., Balakrishna, A.M., Eisenhaber, F., Eisenhaber, B., and Gruber, G. (2014b). Structure, mechanism and ensemble formation of the alkylhydroperoxide reductase subunits AhpC and AhpF from *Escherichia coli*. Acta Crystallogr. D Biol. Crystallogr. *70*, 2848–2862.

Ferreiro, D.U., Komives, E.A., and Wolynes, P.G. (2014). Frustration in biomolecules. Q. Rev. Biophys. *47*, 285–363.

Fiorillo, A., Colotti, G., Boffi, A., Baiocco, P., and Ilari, A. (2012). The crystal structures of the tryparedoxin-tryparedoxin peroxidase couple unveil the structural determinants of *Leishmania* detoxification pathway. Plos Negl. Trop. Dis. *6*, e1781.

Flohe, L., and Harris, J.R. (2007). Introduction. History of the peroxiredoxins and topical perspectives. Subcell. Biochem. *44*, 1–25.

Gillis, J., Schipper-Krom, S., Juenemann, K., Gruber, A., Coolen, S., van den Nieuwendijk, R., van Veen, H., Overkleeft, H., Goedhart, J., Kampinga, H.H., et al. (2013). The DNAJB6 and DNAJB8 protein chaperones prevent intracellular aggregation of polyglutamine peptides. J. Biol. Chem. *288*, 17225–17237.

Gretes, M.C., and Karplus, P.A. (2013). Observed octameric assembly of a *Plasmodium yoelii* peroxiredoxin can be explained by the replacement of native "ball-and-socket" interacting residues by an affinity tag. Protein Sci. *22*, 1445–1452.

Guimaraes, B.G., Souchon, H., Honore, N., Saint-Joanis, B., Brosch, R., Shepard, W., Cole, S.T., and Alzari, P.M. (2005). Structure and mechanism of the alkyl hydroperoxidase AhpC, a key element of the *Mycobacterium tuberculosis* defense system against oxidative stress. J. Biol. Chem. *280*, 25735–25742.

Haley, D.A., Bova, M.P., Huang, Q.L., McHaourab, H.S., and Stewart, P.L. (2000). Small heat-shock protein structures reveal a continuum from symmetric to variable assemblies. J. Mol. Biol. *298*, 261–272.

Hall, A., Sankaran, B., Poole, L.B., and Karplus, P.A. (2009). Structural changes common to catalysis in the Tpx peroxiredoxin subfamily. J. Mol. Biol. *393*, 867–881.

Hanzen, S., Vielfort, K., Yang, J., Roger, F., Andersson, V., Zamarbide-Fores, S., Andersson, R., Malm, L., Palais, G., Biteau, B., et al. (2016). Lifespan control by redox-dependent recruitment of chaperones to misfolded proteins. Cell *166*, 140–151.

Harper, A.F., Leuthaeuser, J.B., Babbitt, P.C., Morris, J.H., Ferrin, T.E., Poole, L.B., and Fetrow, J.S. (2017). An atlas of peroxiredoxins created using an active site profile-based approach to functionally relevant clustering of proteins. PLoS Comput. Biol. *13*, e1005284.

Harris, J.R. (1968). Release of a macromolecular protein component from human erythrocyte ghosts. Biochim. Biophys. Acta *150*, 534–537.

Harris, J.R. (1969). Some negative contrast staining features of a protein from erythrocyte ghosts. J. Mol. Biol. *46*, 329–335.

Harris, J.R., Schröder, E., Isupov, M.N., Scheffler, D., Kristensen, P., Littlechild, J.A., Vagin, A.A., and Meissner, U. (2001). Comparison of the decameric structure of peroxiredoxin-II by transmission electron microscopy and X-ray crystallography. Biochim. Biophys. Acta *1547*, 221–234.

Hartl, F.U., Bracher, A., and Hayer-Hartl, M. (2011). Molecular chaperones in protein folding and proteostasis. Nature *475*, 324–332.

Haslbeck, M., and Vierling, E. (2015). A first line of stress defense: small heat shock proteins and their function in protein homeostasis. J. Mol. Biol. *427*, 1537–1548.

Haslbeck, M., Walke, S., Stromer, T., Ehrnsperger, M., White, H.E., Chen, S., Saibil, H.R., and Buchner, J. (1999). Hsp26: a temperature-regulated chaperone. EMBO J. *18*, 6744–6751.

Haslbeck, M., Weinkauf, S., and Buchner, J. (2019). Small heat shock proteins: simplicity meets complexity. J. Biol. Chem. *294*, 2121–2132.

He, L., and Hiller, S. (2019). Frustrated interfaces facilitate dynamic interactions between native client proteins and holdase chaperones. Chembiochem *20*, 2803–2806.

Hiller, S. (2021). Molecular chaperones and their denaturing effect on client proteins. J. Biomol. NMR *75*, 1–8.

Himiyama, T., Oshima, M., Uegaki, K., and Nakamura, T. (2019). Distinct molecular assembly of homologous peroxiredoxins from *Pyrococcus horikoshii* and *Thermococcus kodakaraensis*. J. Biochem. *166*, 89–95.

Ho, C.T., Grousl, T., Shatz, O., Jawed, A., Ruger-Herreros, C., Semmelink, M., Zahn, R., Richter, K., Bukau, B., and Mogk, A. (2019). Cellular sequestrases maintain basal Hsp70 capacity ensuring balanced proteostasis. Nat. Commun. *10*, 4851.

Hochberg, G.K.A., and Benesch, J.L.P. (2014). Dynamical structure of αβ--crystallin. Prog. Biophys. Mol. Biol. *115*, 11–20.

Horwitz, J. (1992). Alpha-crystallin can function as a molecular chaperone. Proc. Natl. Acad. Sci. U S A *89*, 10449–10453.

Jakob, U., Gaestel, M., Engel, K., and Buchner, J. (1993). Small heat shock proteins are molecular chaperones. J. Biol. Chem. *268*, 1517–1520.

Jang, H.H., Lee, K.O., Chi, Y.H., Jung, B.G., Park, S.K., Park, J.H., Lee, J.R., Lee, S.S., Moon, J.C., Yun, J.W., et al. (2004). Two enzymes in one; two yeast peroxiredoxins display oxidative stress-dependent switching from a peroxidase to a molecular chaperone function. Cell *117*, 625–635.

Jehle, S., van Rossum, B., Stout, J.R., Noguchi, S.M., Falber, K., Rehbein, K., Oschkinat, H., Klevit, R.E., and Rajagopal, P. (2009). αβ-Crystallin: a hybrid solid-state/solution-state NMR investigation reveals structural aspects of the heterogeneous oligomer. J. Mol. Biol. *385*, 1481–1497.

Jehle, S., Vollmar, B.S., Bardiaux, B., Dove, K.K., Rajagopal, P., Gonen, T., Oschkinat, H., and Klevit, R.E. (2011). N-Terminal domain of αβ-crystallin provides a conformational switch for multimerization and structural heterogeneity. Proc. Natl. Acad. Sci. U S A *108*, 6409–6414.

Jeong, W., Bae, S.H., Toledano, M.B., and Rhee, S.G. (2012). Role of sulfiredoxin as a regulator of peroxiredoxin function and regulation of its expression. Free Radic. Biol. Med. *53*, 447–456.

Jiang, Y., Rossi, P., and Kalodimos, C.G. (2019). Structural basis for client recognition and activity of Hsp40 chaperones. Science *365*, 1313–1319.

Jonsson, T.J., Johnson, L.C., and Lowther, W.T. (2008). Structure of the sulphiredoxin-peroxiredoxin complex reveals an essential repair embrace. Nature *451*, 98–101.

Jonsson, T.J., Murray, M.S., Johnson, L.C., Poole, L.B., and Lowther, W.T. (2005). Structural basis for the retroreduction of inactivated peroxiredoxins by human sulfiredoxin. Biochemistry *44*, 8634–8642.

Kamariah, N., Sek, M.F., Eisenhaber, B., Eisenhaber, F., and Gruber, G. (2016). Transition steps in peroxide reduction and a molecular switch for peroxide robustness of prokaryotic peroxiredoxins. Sci. Rep. *6*, 37610.

Karamanos, T.K., Tugarinov, V., and Clore, G.M. (2020). An S/T motif controls reversible oligomerization of the Hsp40 chaperone DNAJB6b through subtle reorganization of a beta sheet backbone. Proc. Natl. Acad. Sci. U S A *117*, 30441–30450.

Karplus, P.A., and Hall, A. (2007). Structural survey of the peroxiredoxins. Subcell. Biochem. *44*, 41–60.

Kim, Y.E., Hipp, M.S., Bracher, A., Hayer-Hartl, M., and Hartl, F.U. (2013). Molecular chaperone functions in protein folding and proteostasis. Annu. Rev. Biochem. *82*, 323–355.

Kitano, K., Kita, A., Hakoshima, T., Niimura, Y., and Miki, K. (2005). Crystal structure of decameric peroxiredoxin (AhpC) from *Amphibacillus xylanus*. Proteins *59*, 644–647.

Kriznik, A., Libiad, M., Le Cordier, H., Boukhenouna, S., Toledano, M.B., and Rahuel-Clermont, S. (2020). Dynamics of a key conformational transition in the mechanism of peroxiredoxin sulfinylation. ACS Catal. *10*, 3326–3339.

Lelj-Garolla, B., and Mauk, A.G. (2006). Self-association and chaperone activity of Hsp27 are thermally activated. J. Biol. Chem. *281*, 8169–8174.

Li, M., Wang, J., Xu, W., Wang, Y., Zhang, M., and Wang, M. (2020). Crystal structure of *Akkermansia muciniphila* peroxiredoxin reveals a novel regulatory mechanism of typical 2-Cys Prxs by a distinct loop. FEBS Lett. *594*, 1550–1563.

Lim, J.C., Choi, H.I., Park, Y.S., Nam, H.W., Woo, H.A., Kwon, K.S., Kim, Y.S., Rhee, S.G., Kim, K., and Chae, H.Z. (2008). Irreversible oxidation of the active-site cysteine of peroxiredoxin to cysteine sulfonic acid for enhanced molecular chaperone activity. J. Biol. Chem. *283*, 28873–28880.

Liu, W., Liu, A., Gao, H., Wang, Q., Wang, L., Warkentin, E., Rao, Z., Michel, H., and Peng, G. (2018). Structural properties of the peroxiredoxin AhpC2 from the hyperthermophilic eubacterium *Aquifex aeolicus*. Biochim. Biophys. Acta Gen. Subj. *1862*, 2797–2805.

Lu, Z., and Cyr, D.M. (1998). The conserved carboxyl terminus and zinc finger-like domain of the co-chaperone Ydj1 assist Hsp70 in protein folding. J. Biol. Chem. *273*, 5970–5978.

Mainz, A., Peschek, J., Stavropoulou, M., Back, K.C., Bardiaux, B., Asami, S., Prade, E., Peters, C., Weinkauf, S., Buchner, J., et al. (2015). The chaperone αβ-crystallin uses different interfaces to capture an amorphous and an amyloid client. Nat. Struct. Mol. Biol. *22*, 898–905.

Mansson, C., Arosio, P., Hussein, R., Kampinga, H.H., Hashem, R.M., Boelens, W.C., Dobson, C.M., Knowles, T.P., Linse, S., and Emanuelsson, C. (2014a). Interaction of the molecular chaperone DNAJB6 with growing amyloid-beta 42 (Abeta42) aggregates leads to sub-stoichiometric inhibition of amyloid formation. J. Biol. Chem. *289*, 31066–31076.

Mansson, C., Kakkar, V., Monsellier, E., Sourigues, Y., Harmark, J., Kampinga, H.H., Melki, R., and Emanuelsson, C. (2014b). DNAJB6 is a peptide-binding chaperone which can suppress amyloid fibrillation of polyglutamine peptides at substoichiometric molar ratios. Cell Stress Chaperones *19*, 227–239.

Mas, G., Burmann, B.M., Sharpe, T., Claudi, B., Bumann, D., and Hiller, S. (2020). Regulation of chaperone function by coupled folding and oligomerization. Sci. Adv. *6*, eabc5822.

Matsumura, T., Okamoto, K., Iwahara, S., Hori, H., Takahashi, Y., Nishino, T., and Abe, Y. (2008). Dimer-oligomer interconversion of wild-type and mutant rat 2-Cys peroxiredoxin: disulfide formation at dimer-dimer interfaces is not essential for decamerization. J. Biol. Chem. *283*, 284–293.

Mayer, M.P., and Bukau, B. (2005). Hsp70 chaperones: cellular functions and molecular mechanism. Cell. Mol. Life Sci. *62*, 670–684.

Meissner, U., Schröder, E., Scheffler, D., Martin, A.G., and Harris, J.R. (2007). Formation, TEM study and 3D reconstruction of the human erythrocyte peroxiredoxin-2 dodecahedral higher-order assembly. Micron *38*, 29–39.

Mizohata, E., Sakai, H., Fusatomi, E., Terada, T., Murayama, K., Shirouzu, M., and Yokoyama, S. (2005). Crystal structure of an archaeal peroxiredoxin from the aerobic hyperthermophilic crenarchaeon *Aeropyrum pernix* K1. J. Mol. Biol. *354*, 317–329.

Mogk, A., Ruger-Herreros, C., and Bukau, B. (2019). Cellular functions and mechanisms of action of small heat shock proteins. Annu. Rev. Microbiol. *73*, 89–110.

Molin, M., Yang, J., Hanzén, S., Toledano, M.B., Labarre, J., and Nyström, T. (2011). Life span extension and H_2O_2 resistance elicited by caloric restriction require the peroxiredoxin Tsa1 in *Saccharomyces cerevisiae*. Mol. Cell *43*, 823–833.

Moon, J.C., Hah, Y.S., Kim, W.Y., Jung, B.G., Jang, H.H., Lee, J.R., Kim, S.Y., Lee, Y.M., Jeon, M.G., Kim, C.W., et al. (2005). Oxidative stress-dependent structural and functional switching of a human 2-Cys peroxiredoxin isotype II that enhances HeLa cell resistance to H_2O_2-induced cell death. J. Biol. Chem. *280*, 28775–28784.

Moore, R.B., Mankad, M.V., Shriver, S.K., Mankad, V.N., and Plishker, G.A. (1991). Reconstitution of Ca^{2+}-dependent K^+ transport in erythrocyte membrane vesicles requires a cytoplasmic protein. J. Biol. Chem. *266*, 18964–18968.

Morgado, L., Burmann, B.M., Sharpe, T., Mazur, A., and Hiller, S. (2017). The dynamic dimer structure of the chaperone trigger factor. Nat. Commun. *8*, 1992.

Nakamura, T., Kado, Y., Yamaguchi, T., Matsumura, H., Ishikawa, K., and Inoue, T. (2010). Crystal structure of peroxiredoxin from *Aeropyrum pernix* K1 complexed with its substrate, hydrogen peroxide. J. Biochem. *147*, 109–115.

Nakamura, T., Mori, A., Niiyama, M., Matsumura, H., Tokuyama, C., Morita, J., Uegaki, K., and Inoue, T. (2013). Structure of peroxiredoxin from the anaerobic hyperthermophilic archaeon *Pyrococcus horikoshii*. Acta Crystallogr. F Struct. Biol. Cryst. Commun. *69*, 719–722.

Nakamura, T., Oshima, M., Yasuda, M., Shimamura, A., Morita, J., and Uegaki, K. (2017). Alteration of molecular assembly of peroxiredoxins from hyperthermophilic archaea. J. Biochem. *162*, 415–422.

Nakamura, T., Yamamoto, T., Abe, M., Matsumura, H., Hagihara, Y., Goto, T., Yamaguchi, T., and Inoue, T. (2008). Oxidation of archaeal peroxiredoxin involves a hypervalent sulfur intermediate. Proc. Natl. Acad. Sci. U S A *105*, 6238–6242.

Nakamura, T., Yamamoto, T., Inoue, T., Matsumura, H., Kobayashi, A., Hagihara, Y., Uegaki, K., Ataka, M., Kai, Y., and Ishikawa, K. (2006). Crystal structure of thioredoxin peroxidase from aerobic hyperthermophilic archaeon *Aeropyrum pernix* K1. Proteins *62*, 822–826.

Nelson, K.J., Parsonage, D., Hall, A., Karplus, P.A., and Poole, L.B. (2008). Cysteine pK(a) values for the bacterial peroxiredoxin AhpC. Biochemistry *47*, 12860–12868.

Nelson, K.J., Perkins, A., Van Swearingen, A.E.D., Hartman, S., Brereton, A.E., Parsonage, D., Salsbury, F.R., Jr., Karplus, P.A., and Poole, L.B. (2018). Experimentally dissecting the origins of peroxiredoxin catalysis. Antioxid. Redox Signal. *28*, 521–536.

Neumann, C.A., Cao, J., and Manevich, Y. (2009). Peroxiredoxin 1 and its role in cell signaling. Cell Cycle *8*, 4072–4078.

Nguyen, J.B., Pool, C.D., Wong, C.Y., Treger, R.S., Williams, D.L., Cappello, M., Lea, W.A., Simeonov, A., Vermeire, J.J., and Modis, Y. (2013). Peroxiredoxin-1 from the human hookworm *Ancylostoma ceylanicum* forms a stable oxidized decamer and is covalently inhibited by conoidin A. Chem. Biol. *20*, 991–1001.

Nielsen, M.H., Kidmose, R.T., and Jenner, L.B. (2016). Structure of TSA2 reveals novel features of the active-site loop of peroxiredoxins. Acta Crystallogr. D Struct. Biol. *72*, 158–167.

Noichri, Y., Palais, G., Ruby, V., D'Autreaux, B., Delaunay-Moisan, A., Nystrom, T., Molin, M., and Toledano, M.B. (2015). In vivo parameters influencing 2-Cys Prx oligomerization: the role of enzyme sulfinylation. Redox Biol. *6*, 326–333.

Pan, A., Balakrishna, A.M., Nartey, W., Kohlmeier, A., Dip, P.V., Bhushan, S., and Gruber, G. (2018). Atomic structure and enzymatic insights into the vancomycin-resistant *Enterococcus faecalis* (V583) alkylhydroperoxide reductase subunit C. Free Radic. Biol. Med. *115*, 252–265.

Papinutto, E., Windle, H.J., Cendron, L., Battistutta, R., Kelleher, D., and Zanotti, G. (2005). Crystal structure of alkyl hydroperoxide-reductase (AhpC) from *Helicobacter pylori*. Biochim. Biophys. Acta *1753*, 240–246.

Parker, A.R., Petluru, P.N., Nienaber, V.L., Badger, J., Leverett, B.D., Jair, K., Sridhar, V., Logan, C., Ayala, P.Y., Kochat, H., et al. (2015). Cysteine specific targeting of the functionally distinct peroxiredoxin and glutaredoxin proteins by the investigational disulfide BNP7787. Molecules *20*, 4928–4950.

Parsonage, D., Youngblood, D.S., Sarma, G.N., Wood, Z.A., Karplus, P.A., and Poole, L.B. (2005). Analysis of the link between enzymatic activity and oligomeric state in AhpC, a bacterial peroxiredoxin. Biochemistry *44*, 10583–10592.

Pastor-Flores, D., Talwar, D., Pedre, B., and Dick, T.P. (2020). Real-time monitoring of peroxiredoxin oligomerization dynamics in living cells. Proc. Natl. Acad. Sci. U S A *117*, 16313–16323.

Perkins, A., Nelson, K.J., Parsonage, D., Poole, L.B., and Karplus, P.A. (2015). Peroxiredoxins: guardians against oxidative stress and modulators of peroxide signaling. Trends Biochem. Sci. *40*, 435–445.

Perkins, A., Nelson, K.J., Williams, J.R., Parsonage, D., Poole, L.B., and Karplus, P.A. (2013). The sensitive balance between the fully folded and locally unfolded conformations of a model peroxiredoxin. Biochemistry *52*, 8708–8721.

Peschek, J., Braun, N., Franzmann, T.M., Georgalis, Y., Haslbeck, M., Weinkauf, S., and Buchner, J. (2009). The eye lens chaperone α-crystallin forms defined globular assemblies. Proc. Natl. Acad. Sci. U S A *106*, 13272–13277.

Phillips, A.J., Littlejohn, J., Yewdall, N.A., Zhu, T., Valery, C., Pearce, F.G., Mitra, A.K., Radjainia, M., and Gerrard, J.A. (2014). Peroxiredoxin is a versatile self-assembling tecton for protein nanotechnology. Biomacromolecules *15*, 1871–1881.

Pineyro, M.D., Pizarro, J.C., Lema, F., Pritsch, O., Cayota, A., Bentley, G.A., and Robello, C. (2005). Crystal structure of the tryparedoxin peroxidase from the human parasite *Trypanosoma cruzi*. J. Struct. Biol. *150*, 11–22.

Prabhu, S., Raman, B., Ramakrishna, T., and Rao Ch, M. (2012). HspB2/myotonic dystrophy protein kinase binding protein (MKBP) as a novel molecular chaperone: structural and functional aspects. PLoS One *7*, e29810.

Radjainia, M., Venugopal, H., Desfosses, A., Phillips, A.J., Yewdall, N.A., Hampton, M.B., Gerrard, J.A., and Mitra, A.K. (2015). Cryo-electron microscopy structure of human peroxiredoxin-3 filament reveals the assembly of a putative chaperone. Structure *23*, 912–920.

Raman, B., and Rao, C.M. (1994). Chaperone-like activity and quaternary structure of α-crystallin. J. Biol. Chem. *269*, 27264–27268.

Rhee, S.G. (2016). Overview on peroxiredoxin. Mol. Cells *39*, 1–5.

Rhee, S.G., Chae, H.Z., and Kim, K. (2005). Peroxiredoxins: a historical overview and speculative preview of novel mechanisms and emerging concepts in cell signaling. Free Radic. Biol. Med. *38*, 1543–1552.

Rhee, S.G., Jeong, W., Chang, T.S., and Woo, H.A. (2007). Sulfiredoxin, the cysteine sulfinic acid reductase specific to 2-Cys peroxiredoxin: its discovery, mechanism of action, and biological significance. Kidney Int. Suppl. S3–S8.

Roger, F., Picazo, C., Reiter, W., Libiad, M., Asami, C., Hanzén, S., Gao, C., Lagniel, G., Welkenhuysen, N., Labarre, J., et al. (2020). Peroxiredoxin promotes longevity and H_2O_2-resistance in yeast through redox-modulation of protein kinase A. eLife *9*, e60346.

Saccoccia, F., Di Micco, P., Boumis, G., Brunori, M., Koutris, I., Miele, A.E., Morea, V., Sriratana, P., Williams, D.L., Bellelli, A., et al. (2012). Moonlighting by different stressors: crystal structure of the chaperone species of a 2-Cys peroxiredoxin. Structure *20*, 429–439.

Saibil, H. (2013). Chaperone machines for protein folding, unfolding and disaggregation. Nat. Rev. Mol. Cell Biol. *14*, 630–642.

Sato, Y., Kojima, R., Okumura, M., Hagiwara, M., Masui, S., Maegawa, K., Saiki, M., Horibe, T., Suzuki, M., and Inaba, K. (2013). Synergistic cooperation of PDI family members in peroxiredoxin 4-driven oxidative protein folding. Sci. Rep. *3*, 2456.

Schröder, E., Isupov, M.N., Naran, A., and Littlechild, J.A. (1999). Crystallization and preliminary X-ray analysis of human thioredoxin peroxidase-B from red blood cells. Acta Crystallogr. *55*, 536–538.

Schröder, E., Littlechild, J.A., Lebedev, A.A., Errington, N., Vagin, A.A., and Isupov, M.N. (2000). Crystal structure of decameric 2-Cys peroxiredoxin from human erythrocytes at 1.7 Å resolution. Structure *8*, 605–615.

Sekhar, A., Velyvis, A., Zoltsman, G., Rosenzweig, R., Bouvignies, G., and Kay, L.E. (2018). Conserved conformational selection mechanism of Hsp70 chaperone-substrate interactions. eLife *7*, e32764.

Soderberg, C.A.G., Mansson, C., Bernfur, K., Rutsdottir, G., Harmark, J., Rajan, S., Al-Karadaghi, S., Rasmussen, M., Hojrup, P., Hebert, H., et al. (2018). Structural modelling of the DNAJB6 oligomeric chaperone shows a peptide-binding cleft lined with conserved S/T-residues at the dimer interface. Sci. Rep. *8*, 5199.

Stocker, S., Maurer, M., Ruppert, T., and Dick, T.P. (2018). A role for 2-Cys peroxiredoxins in facilitating cytosolic protein thiol oxidation. Nat. Chem. Biol. *14*, 148–155.

Stroobants, S., Van Molle, I., Saidi, Q., Jonckheere, K., Maes, D., and Peeters, E. (2019). Structure of the Prx6-subfamily 1-cys peroxiredoxin from *Sulfolobus islandicus*. Acta Crystallogr. F Struct. Biol. Commun. *75*, 428–434.

Tairum, C.A., Jr., de Oliveira, M.A., Horta, B.B., Zara, F.J., and Netto, L.E. (2012). Disulfide biochemistry in 2-cys peroxiredoxin: requirement of Glu50 and Arg146 for the reduction of yeast Tsa1 by thioredoxin. J. Mol. Biol. *424*, 28–41.

Tairum, C.A., Santos, M.C., Breyer, C.A., Geyer, R.R., Nieves, C.J., Portillo-Ledesma, S., Ferrer-Sueta, G., Toledo, J.C., Jr., Toyama, M.H., Augusto, O., et al. (2016). Catalytic Thr or Ser residue modulates structural switches in 2-Cys peroxiredoxin by distinct mechanisms. Sci. Rep. *6*, 33133.

Teixeira, F., Castro, H., Cruz, T., Tse, E., Koldewey, P., Southworth, D.R., Tomas, A.M., and Jakob, U. (2015). Mitochondrial peroxiredoxin functions as crucial chaperone reservoir in *Leishmania infantum*. Proc. Natl. Acad. Sci. U S A *112*, E616–E624.

Teixeira, F., Tse, E., Castro, H., Makepeace, K.A.T., Meinen, B.A., Borchers, C.H., Poole, L.B., Bardwell, J.C., Tomas, A.M., Southworth, D.R., et al. (2019). Chaperone activation and client binding of a 2-cysteine peroxiredoxin. Nat. Commun. *10*, 659.

Vedadi, M., Lew, J., Artz, J., Amani, M., Zhao, Y., Dong, A., Wasney, G.A., Gao, M., Hills, T., Brokx, S., et al. (2007). Genome-scale protein expression and structural biology of *Plasmodium falciparum* and related Apicomplexan organisms. Mol. Biochem. Parasitol. *151*, 100–110.

Voth, W., and Jakob, U. (2017). Stress-activated chaperones: a first line of defense. Trends Biochem. Sci. *42*, 899–913.

Wadley, A.J., Aldred, S., and Coles, S.J. (2016). An unexplored role for peroxiredoxin in exercise-induced redox signalling? Redox Biol. *8*, 51–58.

Wang, X., Wang, L., Wang, X., Sun, F., and Wang, C.C. (2012). Structural insights into the peroxidase activity and inactivation of human peroxiredoxin 4. Biochem. J. *441*, 113–118.

White, H.E., Orlova, E.V., Chen, S., Wang, L., Ignatiou, A., Gowen, B., Stromer, T., Franzmann, T.M., Haslbeck, M., Buchner, J., et al. (2006). Multiple distinct assemblies reveal conformational flexibility in the small heat shock protein Hsp26. Structure *14*, 1197–1204.

Wood, Z.A., Poole, L.B., Hantgan, R.R., and Karplus, P.A. (2002). Dimers to doughnuts: redox-sensitive oligomerization of 2-cysteine peroxiredoxins. Biochemistry *41*, 5493–5504.

Wood, Z.A., Poole, L.B., and Karplus, P.A. (2003a). Peroxiredoxin evolution and the regulation of hydrogen peroxide signaling. Science *300*, 650–653.

Wood, Z.A.S., Harris, R., and Poole, L.B. (2003b). Structure, mechanism and regulation of peroxiredoxins. Trends Biochem. Sci. *28*, 9.

Yang, K.S., Kang, S.W., Woo, H.A., Hwang, S.C., Chae, H.Z., Kim, K., and Rhee, S.G. (2002). Inactivation of human peroxiredoxin I during catalysis as the result of the oxidation of the catalytic site cysteine to cysteine-sulfinic acid. J. Biol. Chem. *277*, 38029–38036.

Yang, Y., Cai, W., Wang, J., Pan, W., Liu, L., Wang, M., and Zhang, M. (2018). Crystal structure of *Arabidopsis thaliana* peroxiredoxin A C119S mutant. Acta Crystallogr. F Struct. Biol. Commun. *74*, 625–631.

Zwirowski, S., Klosowska, A., Obuchowski, I., Nillegoda, N.B., Pirog, A., Zietkiewicz, S., Bukau, B., Mogk, A., and Liberek, K. (2017). Hsp70 displaces small heat shock proteins from aggregates to initiate protein refolding. EMBO J. *36*, 783–796.